

Phase and Charge reentrant phase transitions in two capacitively coupled Josephson arrays with ultra-small junction

Guillermo Ramírez-Santiago

Instituto de Física, Universidad Nacional

Autónoma de México,

Apartado Postal 20-364,

México 01000, D. F., MEXICO

Jorge V. José

Department of Physics and Center for Interdisciplinary

Research on Complex Systems, Northeastern University, 360

Huntington Ave. Boston MA 02115, USA

Abstract

We have studied the phase diagram of two capacitively coupled Josephson junction arrays with charging energy, E_c , and Josephson coupling energy, E_J . Our results are obtained using a path integral Quantum Monte Carlo algorithm. The parameter that quantifies the quantum fluctuations in the i -th array is defined by $\alpha_i \equiv \frac{E_c}{E_{J_i}}$. Depending on the value of α_i , each independent array may be in the semiclassical or in the quantum regime: We find that thermal fluctuations are important when $\alpha \lesssim 1.5$ and the quantum fluctuations dominate when $2.0 \lesssim \alpha$. Vortices are the dominant excitations in the semiclassical limit, while in the quantum regime the charge excitations are important. We have extensively studied the interplay between vortex and charge dominated individual array phases. The phase diagrams for each array as a function of temperature and inter-layer capacitance were determined from results for their helicity modulus, $\Upsilon(\alpha)$, and the inverse dielectric constant, $\epsilon^{-1}(\alpha)$. The two arrays are coupled via the capacitance C_{inter} at each site of the lattices. When one of the arrays is in the quantum regime and the other one is in the semi-classical limit, $\Upsilon(T, \alpha)$ decreases with T , while $\epsilon^{-1}(T, \alpha)$ increases. This behavior is due to a duality relation between the two arrays: e. g. a manifestation of the *gauge invariant capacitive interaction* between vortices in the semiclassical array and charges in the quantum array. We find a *reentrant transition* in $\Upsilon(T, \alpha)$, at low temperatures, when one of the arrays is in the semiclassical limit (i.e. $\alpha_1 = 0.5$) and the quantum array has $2.0 \leq \alpha_2 \leq 2.5$, for the values considered for the interlayer capacitance of $C_{\text{inter}} = 0.26087, 0.52174, 0.78261, 1.04348$ and 1.30435 . Similar results were obtained for larger values of $\alpha_2 = 4.0$ with $C_{\text{inter}} = 1.04348$ and 1.30435 . For smaller values of C_{inter} the superconducting-normal transition was not present. In addition, when $3.0 \leq \alpha_2 < 4.0$, and for all the inter-layer couplings considered above, a *novel* reentrant phase transition occurs in the charge degrees of freedom, i.e. there is a reentrant insulating-conducting transition at low temperatures. Finally, we obtain the corresponding phase diagrams that have some features that resemble those seen in experiment.

PACS numbers: 74.81.Fa, 03.75.Lm, 73.43.Nq, 05.10.Ln

I. INTRODUCTION

This paper considers the phase diagrams of two capacitively coupled Josephson junction arrays (JJA), made of ultrasmall junctions. Two-dimensional JJA have been the subject of many theoretical [1, 2, 3, 4, 5, 6, 7, 8, 9, 10, 11, 12, 13, 14, 15, 16, 17, 18, 19] and experimental [20, 21, 22, 23, 24, 25, 26, 27, 28, 29, 30, 31] studies. Advances in submicrometer technology [25, 26] and in nanolithographic techniques [27, 28] have allowed the fabrication of relatively large arrays made of ultrasmall superconductor-insulator-superconductor Josephson junctions (JJ). The JJ areas may vary from a few microns to submicron dimensions, with self-capacitances $C_s \approx 3 \times 10^{-2}$ fF and nearest neighbor mutual capacitance $C_m \approx 1$ fF. Notice that the mutual capacitance can be at least two orders of magnitude larger than the self-capacitance.

In these arrays there are two competing energies: the Josephson coupling energy, E_J , and the charging energy $E_C = \frac{e^2}{2C_m}$ of the junctions, due to the charge localization in the islands, where e is the electronic charge. In the semiclassical limit, $E_J \gg E_C$, the phase of the superconducting order parameter of the junctions is well defined. The Josephson coupling induces fluctuations in the charge number that produces a supercurrent, where the average Cooper pair number is undefined. In this regime the vortex excitations are pinned by the intrinsic lattice potential and the array is in a superconducting state. In the quantum limit, $E_J \ll E_C$, the electrostatic energy to add one Cooper pair in one of the two islands in a junction is much larger than the thermal energy. The electric field localizes the Cooper pairs in the islands and the quantum fluctuations of the phase of the superconducting order parameter delocalizes the vortex excitations. This charge localization in the junction islands drives the array to an insulating state. The number of Cooper pairs, n , and the phase of the superconducting order parameter, ϕ , obey the Heisenberg's uncertainty principle, $\Delta n \Delta \phi \geq \frac{1}{2}$. This uncertainty relation has been demonstrated experimentally in Al – Al₂O₃ – Al junctions [32].

The superconducting-insulating (S-I) phase transition, induced by the charging energy in arrays of this type, has been experimentally measured as a function of α by groups in Delft [23] and Harvard [24]. Their junction sizes had constant values, while they varied the normal state junction resistance to change the Josephson coupling energy. This allowed

them to fabricate arrays with α in the range $[0.13 - 4.55]$ [23], or as high as 33 [24]. JJA have also been studied in connection with quantum phase transitions [17]. The JJA have the advantage, over films, that their internal structure can be carefully controlled experimentally. The drawback is that the array sizes are limited by fabrication constraints. There is a large literature studying the phase transition structure of one JJA with ultra small junctions as the temperature, the external magnetic field and α are varied (for a comprehensive recent review see [25]).

A novel experimental system composed of *two capacitively coupled JJA* made of ultrasmall junctions was discussed in a paper by the Delft group [26], in which each array was produced with different α parameters. Initial theoretical studies of this system were started in [33], [34] and in [35]. In this paper we study the phase diagram of this very interesting system. The Hamiltonian describing the coupled arrays can be formally written as $\hat{\mathcal{H}} = \hat{H}_J(1) + \hat{H}_J(2) + \hat{H}_C(1, 2)$, where the $\hat{H}_J(i)$ denote the Josephson Hamiltonians for each array, and $H_C(1, 2)$ describes the two arrays capacitive interactions. $H_C(1, 2)$ includes the total charging energy matrix, which includes the self- and mutual capacitive terms in each plane, plus the arrays interaction due to the ultrasmall nearest neighbor capacitive coupling between them. This Hamiltonian is more complicated to study than the single array problem studied before [23, 25]. Here each array is described by the ratio $\alpha_i = (E_{C_i}/E_{J_i})$ ($i = 1, 2$), with the mutual array capacitive coupling denoted by α_{int} . In the $\alpha_i \ll 1$ limit, the i -th array is dominated by localized vortex excitations, V_i , while the Cooper pair excess charge excitations, Q_i , are in a superconducting state. In the $\alpha_i \gg 1$ regime, the system has the Q_i 's localized in an insulating state while the V_i 's are delocalized. There are different parameter regimes that can be studied. Here we consider in detail the case when one array is V dominated and the other array Q dominated. Using the Villain approximation and duality transformations [36], it was shown [33, 34, 35] that the interaction between vortices and charges has a minimal gauge coupling form, and that the interaction is sharply localized in space: A vortex and a Cooper pair interact only if they are located at the same site in both arrays. In previous studies an effective Hamiltonian was derived, in terms of V_1 and Q_2 , which shows a high degree of dual symmetry, with the $V_1 \longleftrightarrow Q_2$ interaction expressed as *a capacitively induced minimal gauge like coupling* [15, 33, 34, 35].

We used a path integral Quantum Monte Carlo algorithm to further study the behavior

of this system. We calculated the phase diagram described in terms of the vortex helicity modulus, Υ , and the charge inverse dielectric constant, ϵ^{-1} , as a function of α and temperature. We find that as α varies there are different *novel* reentrant phase transitions seen in Υ and ϵ^{-1} . These re-entrances indicate transitions between SC-N, SC-I and I-N phases. The layout of the paper is as follows: In section II we define and explain the model of interest and the path integral formalism to evaluate its partition function, as well as the physical quantities that are calculated to characterize the behavior of the model. In section III we present and discuss the results of our calculations and finally, in section IV, we summarize our main findings and present our conclusions.

II. THE MODEL AND ITS PATH INTEGRAL REPRESENTATION

In this section we define the model that describes two JJA made of ultra small junctions capacitively coupled at each lattice site. The parameter values used in the simulations correspond to those present in the experimental samples fabricated and studied at Delft [23]. The dimensions of the experimental arrays were $L_x = 230$ and $L_y = 60$, with intra-layer mutual capacitance of $C_m = 2.3$ fF, and inter-layer capacitance $C_{\text{int}} = 0.6$ fF.

The model Hamiltonian is defined by [35],

$$\begin{aligned} \mathcal{H} = & \frac{Q^2}{2} \sum_{\langle \vec{r}_1, \vec{r}_2 \rangle} \sum_{\mu=1, \nu=1}^2 \mathbf{n}_\mu(\vec{r}_1) \tilde{\mathbf{C}}_{\mu, \nu}^{-1}(\vec{r}_1, \vec{r}_2) \mathbf{n}_\nu(\vec{r}_2) + E_{J_1} \sum_{\langle \vec{r}_1, \vec{r}_2 \rangle} \left(1 - \cos(\phi_1(\vec{r}_1) - \phi_1(\vec{r}_2)) \right) \\ & + E_{J_2} \sum_{\langle \vec{r}_1, \vec{r}_2 \rangle} \left(1 - \cos(\phi_2(\vec{r}_1) - \phi_2(\vec{r}_2)) \right), \end{aligned} \quad (1)$$

where the sums are over nearest neighbors, and μ and ν label the matrix elements of the mutual capacitive interactions. \vec{r}_1 and \vec{r}_2 denote the positions of the junctions in arrays 1 and 2, respectively. The operator $\mathbf{n}_\mu(\vec{r}_1)$, for the number of Cooper pairs, and the phase of the superconducting order parameter $\hat{\phi}_\nu(\vec{r}_2)$, satisfy the Heisenberg commutation relations, $[\mathbf{n}_\mu(\vec{r}_1), \hat{\phi}_\nu(\vec{r}_2)] = -i\delta_{\vec{r}_1, \vec{r}_2} \delta_{\mu, \nu}$. The charge carried by the Cooper pairs is $Q = 2e$, and E_{J_1} and E_{J_2} are the Josephson coupling constants within each array. $\tilde{\mathbf{C}}_{\mu, \nu}^{-1}$ is the electric field propagator and its inverse, $\mathbf{C}_{\mu, \nu}$, is the block matrix representing the geometric capacitance. In what follows we will use the notation $\mathbf{C}_{\mu, \mu} = \mathbf{C}_\mu$ to denote the diagonal capacitance

matrix. The block matrices are given by,

$$\mathbf{C}_{\mu,\nu}(\vec{r}_1, \vec{r}_2) = \begin{cases} (C_{s,\mu} + zC_{m,\mu} + C_{\text{int}}), & \text{if } \mu = \nu \text{ and } \vec{r}_1 = \vec{r}_2, \\ -C_{m,\mu}, & \text{if } \mu = \nu \text{ and } \vec{r}_1 = \vec{r}_2 \pm \vec{u}, \\ -C_{\text{int}}, & \text{if } \mu \neq \nu \text{ and } \vec{r}_1 = \vec{r}_2, \\ 0, & \text{otherwise.} \end{cases} \quad (2)$$

Here \vec{d} is a unit vector and z is the lattice coordination number. The off-diagonal blocks are written as $-C_{\text{int}} \mathbf{I}_{N,N}$ with \mathbf{I} the identity matrix and N the size of the arrays. The block matrix elements in the Hamiltonian in Eq. (1) are written as [35],

$$\begin{aligned} \tilde{\mathbf{C}}_{1,1} &= \mathbf{C}_1^{-1} [\mathbf{I} - C_{\text{int}}^2 \mathbf{C}_2^{-1} \mathbf{C}_1^{-1}]^{-1}, \\ \tilde{\mathbf{C}}_{2,2} &= \mathbf{C}_2^{-1} [\mathbf{I} - C_{\text{int}}^2 \mathbf{C}_1^{-1} \mathbf{C}_2^{-1}]^{-1}, \\ \tilde{\mathbf{C}}_{1,2} &= C_{\text{int}} \mathbf{C}_1^{-1} \mathbf{C}_2^{-1} [\mathbf{I} - C_{\text{int}}^2 \mathbf{C}_1^{-1} \mathbf{C}_2^{-1}]^{-1}, \\ \tilde{\mathbf{C}}_{2,1} &= C_{\text{int}} \mathbf{C}_2^{-1} \mathbf{C}_1^{-1} [\mathbf{I} - C_{\text{int}}^2 \mathbf{C}_2^{-1} \mathbf{C}_1^{-1}]^{-1}. \end{aligned} \quad (3)$$

To evaluate the partition function, Ξ , we can calculate the trace over the phase operators $\hat{\phi}$ or over the trace of the number operators $\hat{\mathbf{n}}$. The path integral representation of Ξ can be obtained using the states [37],

$$\langle n(\vec{r}_1) | \phi(\vec{r}_2) \rangle = \frac{\exp[in(\vec{r}_1)\phi(\vec{r}_2)]}{\sqrt{2\pi}} \delta_{\vec{r}_1, \vec{r}_2}. \quad (4)$$

Following the steps outlined in reference [15], we obtain the lattice path integral representation of the partition function,

$$\begin{aligned} \Xi &= \prod_{\tau=0}^{L_\tau-1} \prod_{\vec{r}} \sum_{n(\tau, \vec{r})} \int_0^{2\pi} \frac{d\phi(\tau, \vec{r})}{2\pi} \exp \left\{ - \int_0^{\beta\hbar} d\tau \left[\sum_{\vec{r}_1, \vec{r}_2} \frac{Q^2}{2} n(\tau, \vec{r}_1) \mathbf{C}^{-1}(\vec{r}_1, \vec{r}_2) n(\tau, \vec{r}_2) \right. \right. \\ &\quad \left. \left. + i \sum_{\vec{r}} n(\tau, \vec{r}) \frac{d\phi}{d\tau}(\tau, \vec{r}) + E_J \sum_{\langle \vec{r}_1, \vec{r}_2 \rangle} [1 - \cos(\phi(\tau, \vec{r}_1) - \phi(\tau, \vec{r}_2))] \right] \right\}. \end{aligned} \quad (5)$$

Eq. (5) involves the phase $\phi(\tau, \vec{r})$ and the charge integer fields $n(\tau, \vec{r})$ as statistical variables, in a three dimensional lattice with two spatial dimensions $L_x \times L_y$, and one imaginary time dimension, L_τ . The angular phases $\phi(\tau, \vec{r}) \in [0, 2\pi]$ are defined at the nodes of the lattice with periodic boundary conditions in the x and y space dimensions. The integer

fields, $n(\tau, \vec{r})$, lie in the bonds between two consecutive nodes along the imaginary time axis τ , and they can take any integer values. The quantization condition in Ξ is imposed in terms of the periodic boundary conditions $\phi(L_\tau, \vec{r}) = \phi(0, \vec{r})$. The $L_\tau \rightarrow \infty$ limit has been formally taken to replace the sum over imaginary time by its integral. This Ξ representation is amenable to numerical calculations in comparison to its operator representation.

The arrays can be in a superconductor, insulator, or normal states, depending on the values of T , α and C_{int} . To characterize the superconducting or normal state behavior we calculated the helicity modulus, Υ , for each array,

$$\Upsilon = \left. \frac{\partial^2 \mathcal{F}}{\partial k^2} \right|_{k=0}. \quad (6)$$

Υ measures the energy needed to carry out a phase twist between the boundaries of the array along the \vec{k} direction. The helicity modulus is proportional to the superfluid density per unit mass ρ_s ,

$$\rho_s(T) = \frac{1}{V} \left(\frac{ma}{\hbar} \right) \Upsilon(T). \quad (7)$$

Here a is the lattice spacing, m the Cooper pair mass, and V the volume. Combining Eqs. (5) and (6), we obtain the path integral representation of the helicity modulus when the twist is along the \vec{x} axis [15],

$$\begin{aligned} \frac{1}{E_{J_\nu} L_x L_y} \Upsilon_\nu^x(T) = & \frac{1}{L_x L_y L_\tau} \left[\left\langle \sum_{\tau=0}^{L_\tau-1} \sum_{\vec{r}_\nu} \cos \left[\phi(\tau, \vec{r}_\nu) - \phi(\tau, \vec{r}_\nu + \hat{x}) \right] \right\rangle \right. \\ & - \frac{E_{J_\nu} \beta}{L_\tau} \frac{E_{J_\nu} \beta}{L_\tau} \left\{ \left\langle \left(\sum_{\tau=0}^{L_\tau-1} \sum_{\vec{r}_\nu} \sin \left[\phi(\tau, \vec{r}_\nu) - \phi(\tau, \vec{r}_\nu + \hat{x}) \right] \right)^2 \right\rangle \right. \\ & \left. \left. - \left\langle \sum_{\tau=0}^{L_\tau-1} \sum_{\vec{r}_\nu} \sin \left[\phi(\tau, \vec{r}_\nu) - \phi(\tau, \vec{r}_\nu + \hat{x}) \right] \right\rangle^2 \right\} \right]. \quad (8) \end{aligned}$$

The charge coherence in the arrays is determined by the inverse dielectric constant ε^{-1} , defined as,

$$\varepsilon^{-1} = \lim_{\vec{q} \rightarrow 0} \left[1 - \frac{Q^2}{k_B T} \frac{1}{\mathbf{C}(\vec{q})} \langle n(\vec{q}) n(-\vec{q}) \rangle \right]. \quad (9)$$

Combining Eqs. (5) and (9), as well as Fourier transforming the capacitance matrix and the charge number operator [15], we can write the path integral representation of the correlation function $\langle n(\vec{r}_1) n(\vec{r}_2) \rangle$ as,

$$\langle n(\vec{r}_1) n(\vec{r}_2) \rangle = \frac{1}{\beta Q^2} \mathbf{C}(\vec{r}_1, \vec{r}_2) + \left(\frac{2\pi}{\beta L_\tau} \right)^2 \sum_{\vec{r}_3, \vec{r}_4} \mathbf{C}(\vec{r}_1, \vec{r}_3) \mathbf{C}(\vec{r}_2, \vec{r}_4) \langle m(\vec{r}_3), m(\vec{r}_4) \rangle. \quad (10)$$

Substituting this result in Eq.(9) yields the inverse dielectric constant expression

$$\epsilon^{-1} = \lim_{\vec{k} \rightarrow 0} \left[\frac{(2\pi)^2}{\beta Q^2} \mathbf{C}(\vec{k}) \langle |m(\vec{k})|^2 \rangle \right]. \quad (11)$$

In these equations the path integral representation of the integer fields $m(\vec{r})$'s is $m(\vec{r}) = \sum_{\tau=0}^{L_\tau-1} m(\tau, \vec{r})$. It is important to note that the path integral representation of ϵ^{-1} in Eq. (11) is not exactly the inverse dielectric function of a gas of Cooper pairs, since it depends on the discretization of the imaginary time axis in L_τ slices. Nonetheless, we expect that it contains most of the relevant information of the dielectric properties of the gas of Cooper pairs in the arrays.

III. RESULTS AND DISCUSSION

A. Parameter values in the simulations

To carry out the Monte Carlo moves in the phases we used the standard Metropolis algorithm. To speed up the calculations, we replace the $U(1)$ continuous symmetry in the phases by a discrete \mathbf{Z}_N subgroup [2]. Using $N = 5000$ has proved to yield good results. Discretizing the phases has the advantage of using integer arithmetic that allows building cosine tables for the Boltzmann factors in the partition function. This simplification cannot be used for the integer fields, except when $C_m = 0$, in which case the $m(\tau, \vec{r})$ fields can be summed up exactly. This approach allows to build up look up tables that introduce an adequate effective potential [15].

Once the system reaches thermal equilibrium after N_{ther} (between 10^3 and 10^4) MC sweeps, the thermodynamic averages of interest were calculated. A measure was taken after N_{sweeps} passes through the arrays updating the phases, and M_{sweeps} passes updating the integer fields. In the semi-classical limit, $\alpha \ll 1$, and we needed to consider $N_{\text{sweeps}} = 1$ and $M_{\text{sweeps}} = 1$ at high temperatures ($T > 0.4$), and $N_{\text{sweeps}} = 4$ and $M_{\text{sweeps}} = 4$ at low temperatures ($T < 0.4$). In the quantum limit, $\alpha > 1$, we took $N_{\text{sweeps}} = 4$ and $M_{\text{sweeps}} = 4$, at high temperatures, and $N_{\text{sweeps}} = 10$ and $M_{\text{sweeps}} = 10$ at low temperatures. These parameter values were chosen to minimize the decorrelation times due to the long range charge interactions. Proceeding in this way we carried out averages over 16384 MC steps

at high temperatures and 32768 at low temperatures. Error bars were calculated using the biased reduction method described in reference [38].

We studied the helicity modulus and the inverse dielectric constant for each array as a function of temperature, α , and the ratio of the inter-layer self capacitance to the intralayer mutual capacitance, $\frac{C_{\text{int}}}{C_{\text{m}}}$. The reduced temperature was varied in the range $[0.05, 1.0]$ in 0.05 steps at high T 's and 0.025 steps at low T 's. To study the transition between the semi-classical and quantum states, the quantum parameter in one array was kept fixed at $\alpha_1 = 0.5$ while we varied the quantum parameter of the second array taking values, $\alpha_2 = 0.5, 1.0, 1.25, 1.50, 2.0, 2.5, 3.0$, and 4.0. In addition, the capacitance ratios were integer multiples of the Delft's experimental parameters [23]: $\frac{C_{\text{int}}}{C_{\text{m}}} = \kappa \times 0.26087$, with $\kappa = 1, 2, 3, 4$, and 5. The values chosen for this ratio allowed us to study the effects of the capacitive coupling between the arrays, going from weak coupling, to the strong coupling regime when $\kappa \geq 3$. The simulations were carried out in lattice sizes $L_x \times L_y = 32 \times 32$ and $L_\tau = 32$, for $0.5 \leq \alpha \leq 2.0$, and L_τ up to 96 for higher values $2.0 < \alpha \leq 4.0$. The larger the value α the larger the imaginary time axis had to be. For the L_τ values chosen we obtained reliable results, with negligible finite size effects along the imaginary time axis.

B. Results for Υ and ϵ^{-1}

In this section we present and discuss the results for $\Upsilon_{1,2}$ and $\epsilon_{1,2}^{-1}$ for different values of the quantum parameter α_2 while $\alpha_1 = 0.5$ was kept fixed. We start considering the case when both arrays are in the semi-classical regime, $\alpha_1 = 0.5$ and $\alpha_2 = 1.0$ and $0.26087 \leq C_{\text{int}} \leq 1.30435$. The corresponding results are not shown explicitly here, however, we briefly describe them to compare, where appropriate, with previous studies. We found that at low temperature $\Upsilon_{1,2}$ are finite –SC phase– with $\Upsilon_1 > \Upsilon_2$, with small thermal fluctuations. Both quantities decreased monotonically down to zero as temperature increased. For $T \geq T_{\text{sc}}(\alpha_{1,2})$ they were equal to zero indicating that the arrays were in the normal phase. The superconductor to normal (SC-N) transition temperature, $T_{\text{SC}}(\alpha)$, shifted downwards as the charging energy increased. Around this transition temperature the fluctuations of Υ became larger. Since the arrays were in the semiclassical regime the charges did not play an important role in the behavior of the system, except for the small decrease in phase

coherence, and we obtained, $\varepsilon_{1,2}^{-1} = 0$, in the whole temperature range. These results for the two coupled arrays are in agreement with previous studies for one array [2, 3, 4, 15]. The results described here indicate that $T_{SC}(\alpha)$ was weakly affected by the interlayer capacitive coupling.

In Fig. 1 we show the helicity modulus –upper panels– and the inverse dielectric constant –lower panels– of each array as a function of temperature when $\alpha_1 = 0.5$ and $\alpha_2 = 2.5$, for low and high values of $\frac{C_{\text{int}}}{C_{\text{m}}}$. The dependence of the SC-N phase boundary $T_{SC}(\alpha)$ on C_{int} will be shown and discussed later. In figure 1 we see that the second array starts to develop charge coherence: At very low temperatures the inverse dielectric constant of 1, although small, it has increased while the phase coherence of the second array decreased, as shown by the reduced value of the helicity modulus. This behavior confirms the dual behavior between vortices in one array and charges in the other one, due to their *gauge interaction*, as predicted in reference [35]. There, an effective action was written in terms of four interacting imaginary time Coulomb-like gases. The effective Hamiltonian was shown to be dually symmetric between charge and vorticity with complicated kernels. In the simplest case, where one array has one vortex and the other one charge, their interaction has a minimal gauge coupling that is proportional to the site coupling capacitance between the arrays. As a consequence of this *gauge capacitive interaction*, the fluctuations in the helicity modulus and the inverse dielectric constant are much stronger than those observed in the semi-classical limit in a single array. Nonetheless, the quantum fluctuations in the second array are not sufficiently strong to significantly affect the semi-classical behavior of the first array. This indicates that the *gauge interaction* between vortex and charge Coulomb gases is weak. On the other hand, it also found that as C_{int} increases the charge coherence of the second array decreases, restoring its phase coherence. In addition there appears to be a reentrant phase transition in the second array at low temperatures, as suggested by the concave curvature of its helicity modulus and the slight convex curvature of its inverse dielectric constant. This picture becomes more evident when increasing further the charging energy in the second array, to $\alpha_2 = 3.0$, while keeping $\alpha_1 = 0.5$. The results are shown in Fig. 2. When $\frac{C_{\text{int}}}{C_{\text{m}}} = 0.52174$, as the system cools down, array 2 undergoes a SC-N phase transition at $T \simeq 0.35$, followed by a reentrant N-SC transition at $T \simeq 0.25$. In addition, we also observe that at $T \simeq 0.45$ the charge coherence increases significantly and then

decreases at $T \simeq 0.15$. This suggests an insulating to normal reentrant transition. Once again, this is a manifestation of the dual character between the charge and phase degrees of freedom in the two arrays as well as the *gauge interaction* between the vortex and charge Coulomb gases. As the interaction capacitance increases further to $\frac{C_{\text{int}}}{C_{\text{m}}} = 0.78261$, the reentrant transition in the phase degrees of freedom is less evident, but it is still present. A similar situation is observed in the charges degrees of freedom. Increasing further the arrays interaction capacitance improves the phase coherence of the arrays at the expense of their charge coherence. Note that the thermal fluctuations are strong in the phase and in the charge degrees of freedom for the array parameters considered here. In spite of the capacitive interaction between arrays 1 and 2, the behavior in array 2 does not affect significantly the behavior of array 1. When the quantum parameter of array 2 is sufficiently large, $\alpha_2 = 4.0$, the quantum effects become dominant, and the charge degrees of freedom destroy the phase coherence when $\frac{C_{\text{int}}}{C_{\text{m}}} = 0.52174$ and 0.78261 . This behavior is shown in figure 3. For this value of α_2 we needed to consider $L_\tau = 96$ for array 2 to get meaningful results. We found no transition at all in the phases, but we do get a sharp N-I transition for the charges, although the fluctuations in those degrees of freedom are rather large. Increasing C_{int} further leads to a different scenario. For $\frac{C_{\text{int}}}{C_{\text{m}}} = 1.04348$, a SC phase appears in the temperature range $0.25 \leq T \leq 0.45$, followed by an insulating phase at lower temperatures. For $\frac{C_{\text{int}}}{C_{\text{m}}} = 1.30435$ we obtain a similar situation. In this case the phase coherence is greater than for the previous values of the interaction capacitance parameter. These results are shown in figure 4.

As pointed out in section II, when the quantum parameter, $\alpha \geq 1$, the numerical evaluation of the path integral representation of ε^{-1} –Eq. (11)– depends importantly on the time slice discretization of the imaginary time axis, that is, there are finite size effects. To ascertain this situation we calculated $\Upsilon(T)$ and $\epsilon^{-1}(T)$ for four different imaginary time axis lengths, $L_\tau = 48, 64, 96$, and 128 . In figures 5(a),(b) we show the results of these calculations for $\Upsilon_i(T)$, $i = 1, 2$ when $\frac{C_{\text{int}}}{C_{\text{m}}} = 1.30435$ with $\alpha_1 = 0.5$, and $\alpha_2 = 4$. We see that $\Upsilon_1(T)$ shows no finite size effects since the data for different values of L_τ for each T fall on top of each other. There are very small finite size effects for those temperatures close to the SC-N transition temperature. However, $\Upsilon_2(T)$ shows important finite size effects in the temperature region where the reentrant transition sets in. This reentrance becomes better defined, and its behavior becomes smoother for $L_\tau \geq 96$. Similarly, the SC-I temperature

shifts slightly to lower temperatures for $L_\tau \geq 96$, while the N-SC temperature remains about the same. On the other hand, $\epsilon_1^{-1}(T) = 0$ in the whole temperature range considered. This is not unexpected since array 1 is in the semi-classical regime ($\alpha_1 = 0.5$), and the role of the charge degrees of freedom is negligible. Because of this we do not show ϵ_1^{-1} in figures 5. Nonetheless, $\epsilon_2^{-1}(T)$ is sensitive to the L_τ length axis, as can be seen in figure 5(c). In this case, we see that the insulating phase sets in at the temperature boundary $T_{SC-I}(L_\tau)$. For $L_\tau \geq 96$ it shifts slightly to lower temperatures. We also see strong fluctuations in the inverse dielectric constant at about T_{SC-I} . For other values of $\frac{C_{\text{int}}}{C_m}$, and α_2 , the results are less significant. Although we did not see a clear saturation of $\epsilon_2^{-1}(T)$ at the reentrance transition for the two largest values of L_τ we were able to minimize the finite size effects along the imaginary time length. Carrying out calculations using larger imaginary time axis becomes very demanding from the computational point of view.

C. Phase diagrams

Here we present the cumulative results from the estimation of the critical temperatures from our $\Upsilon(T, \alpha)$ and $\epsilon^{-1}(T, \alpha)$ calculations that provide the phase boundaries for the SC-N and I-N phase transitions. In array 1 the quantum parameter $\alpha_1 = 0.5$, is kept fixed, while α_2 was varied in the interval $1.0 \leq \alpha_2 \leq 4.0$, in $\Delta\alpha_2 = 0.5$ steps, for each one of the values of C_{int}/C_m . The transition temperatures were estimated from the behavior of Υ and ϵ^{-1} as functions of temperature, for each value of α_2 . In the classical arrays, according to the Berezinskii-Kosterlitz-Thouless (BKT) theory, the critical SC-N temperature occurs at the intercept of the helicity modulus with a straight line with slope $\frac{2}{\pi}$. In the quantum arrays it has been shown experimentally that in the limit $C_s/C_m \rightarrow 0$ there is a crossover from a conducting to an insulating phase [22, 24, 29]. Due to the finite size of the experimental arrays there is a rounding of the transitions, because the screening length is shorter than the size of the arrays [23]. Theoretically it has been argued that for any finite screening length the phase transition is washed out even in arrays of infinite size [39]. This happens because in the BKT scenario the SC-N transition crucially depends on the unscreened nature of the logarithmic interaction between vortex pairs [36, 40]. Nonetheless, it has been recently shown [18, 19] that even in the regime of strong quantum fluctuations the data for $\Upsilon(T)$, at

low temperatures, can be very well fitted to the Kosterlitz's renormalization group equations in a finite size analysis of Υ . In spite of the theoretical and the experimental differences in estimating the transition temperatures, here we will use the BKT theory since we have not carried out a detailed finite size analysis. When there is a low temperature reentrant phase transition, the transition temperature is determined from the temperature at which the physical quantity of interest vanishes, as is done with the arrays's electric resistance in experiments. The error bars in the transition temperatures were estimated taking into account the size of the temperature variation step, ΔT , in the calculations. Since $\Delta T = 0.05$, then the error bars in the transition temperatures of the phase boundaries are $\delta T_c = 0.05$.

In figure 6 we show the phase diagrams T_c versus α_2 for the phase and charge degrees of freedom for arrays 1 and 2, when $C_{\text{int}}/C_m = 0.52174$. We see that the SC-N temperature boundary of the semiclassical array 1 remains almost unchanged as a function of α_2 , with $T_c \simeq 0.85$. The SC-N phase boundary of array 2, however, changes significantly as α_2 increases. The transition temperature decreases monotonically and it extrapolates to zero at $\alpha_2 = 4$. At this α_2 value the second array is fully in the quantum regime. Similar results were obtained for $C_{\text{int}}/C_m = 0.26087$. It was also found that the I-N phase boundaries of the arrays are qualitatively similar for $1 \leq \alpha_2 \leq 2.5$ with $C_{\text{int}}/C_m = 0.26087$ and 0.52174 . That is, for array 1 $T_{\text{IC}}(\alpha_2) = 0$, and for array 2 the I-N transition temperature increases monotonically and reaches a maximum at $\alpha_2 = 2.5$. However, when array 2 is in the quantum regime, $\alpha_2 > 2.5$, the situation is different. There we found that the I-N boundary of array 1 is equal to zero when $C_{\text{int}}/C_m = 0.26087$. Increasing this quantity up to 0.52174 , yields a nonzero and monotonically increasing $T_{\text{IC}}(\alpha_2)$. For array 2 with $C_{\text{int}}/C_m = 0.26087$ we found that the $T_{\text{IC}}(\alpha_2)$ decreases slowly and for $3 \leq \alpha_2 \leq 4$ it becomes constant, $T_{\text{IC}} \simeq 0.3$. For larger values of the interaction parameter, $C_{\text{int}}/C_m = 0.52174$, the I-N phase boundary decreases down to zero for $3.0 \leq \alpha_2 \leq 4.0$, indicating the existence of a reentrant *novel* phase transition. The results for $C_{\text{int}}/C_m = 0.52174$ are plotted in figure 6. For $C_{\text{int}}/C_m = 0.78261$, the SC-N phase diagram for array 2, and the I-N phase diagram of both arrays, are modified slightly. The $T_{\text{SC-N}}$ boundary of array 2 decreases at about the same rate when $1.0 \leq \alpha_2 \leq 3.0$ for the values of C_{int}/C_m given above. Nonetheless, the transition temperature for $\alpha_2 = 4.0$ is not zero, instead, it moves upwards. $T_{\text{SC-N}}$ may be approximated by a straight line for the whole interval of α_2 considered here. The I-N boundary, it increases monotonically from $\alpha_2 = 1.25$

up to $\alpha_2 = 2.0$, where it reaches a maximum and then slowly decreases appearing to reach a minimum at $\alpha_2 = 3.0$. Above this value it increases slowly. These results are not shown here since they are similar to those in Fig. 7. A further increase in the coupling capacitance between the arrays to, $C_{\text{int}}/C_{\text{m}} = 1.04348$, does not change the SC-N and the I-N boundaries of array 1, but it changes the SC-N phase diagram for array 2, and the I-N phase diagram of both arrays. The SC-N transition temperature of array 2 decreases linearly as a function of α_2 , while the I-N boundary increases monotonically in the temperature range $1.0 \leq T \leq 2.5$. It reaches a maximum at $T = 2.5$ and then decreases slowly up to $\alpha_2 = 3.0$, where it has a minimum and then increases again up to $\alpha_2 = 4.0$. Note that the position of the maximum is shifted to higher values of α_2 , and the transition temperature at $\alpha_2 = 4.0$ shifts downwards compared to the previous value of $C_{\text{int}}/C_{\text{m}}$. When $C_{\text{int}}/C_{\text{m}}$ is at the highest value considered here, 1.30305, the SC-N boundaries of arrays 1-2 become straight lines. The former has zero slope and the latter shows a negative slope, i.e. the SC-N transition temperature of array 2 decreases linearly as α_2 increases. On the other hand, the I-N boundary of array 1 starts as a horizontal straight line for $1 \leq \alpha_2 \leq 1.5$ then increases reaching a maximum at $\alpha_2 = 2.5$, then decreasing monotonically down to zero at $\alpha_2 = 4.0$. These results suggest, again, the existence of a *reentrant transitions* in array 2 when it is in the quantum regime. In contrast, the I-N boundary of array 2 is a horizontal line at $T = 0$, for $1 \leq \alpha_2 \leq 3.0$, and $T_{\text{I-N}}(\alpha)$ becomes nonzero for $\alpha_2 > 3.0$.

The structure of the phase diagrams indicate that by increasing the capacitive coupling between arrays and increasing the α_2 parameter one can induce novel reentrant phase transitions not only in the phase degrees of freedom but also in the charge freedoms. This is a situation that does not occur in single JJA.

IV. CONCLUSIONS

We have carried out extensive path integral quantum MC simulations of two capacitively coupled JJA with ultra small junctions. One in the semiclassical limit and the other in the quantum regime. We studied the behavior of the helicity modulus and the inverse dielectric constant as a function of temperature for different values of the interlayer capacitances. When both arrays are in the semiclassical regime, regardless of the interlayer coupling consid-

ered here, each array shows a SC-N transition at finite temperatures. For these semiclassical arrays the charge degrees of freedom contribution is negligible and there is no I-N transition at finite temperatures. As array 2 enters the quantum regime ($2.0 \leq \alpha_2 \leq 2.5$), a SC-N reentrant phase transition appears and the fluctuations in Υ_2 and ϵ^{-1} become significantly larger due to quantum fluctuations as explained in references [18, 19]. At the same time the quantum array starts to develop charge coherence with an finite temperature I-N transition. This scenario occurred for all the values of the interlayer coupling considered here. As array 2 becomes more quantum ($3.0 \leq \alpha_2 < 4.0$), and for all the interlayer couplings considered, *reentrant transitions* occur not only in the phase degrees of freedom, but also in the charges degrees of freedom. When $\alpha_2 = 4.0$, the SC-N transition is washed out for values of the interlayer coupling $C_{\text{int}}/C_{\text{m}} \leq 0.78261$, having only an I-N transition. Increasing further the interlayer coupling yields a SC-N reentrant phase transition at low temperatures for $0.20 \lesssim T \lesssim 0.5$, together with the usual I-N phase transition for the charges. These scenarios can be understood as a manifestation of the *gauge interactions between the phase degrees of freedom and the charge degrees of freedom that are present in each array*. The latter results depend on the values of the quantum parameters. Finally, we showed a series of interesting phase diagrams for both arrays where we found some resemblance to the reentrant-like behavior observed experimentally by the Delft's group in 2D JJA with charging energy [23, 31].

V. ACKNOWLEDGEMENTS

GRS would like to acknowledge partial financial support from CONACYT-MEXICO through contract 25298-E and from DAGAPA-UNAM contract IN110103. JVJ thanks NSF for partial financial support.

-
- [1] J. V. José, Phys. Rev. B **29**, 2836 (1984).
- [2] L. Jacobs, J. V. José and M. A. Novotny, Phys. Rev. Lett. **53**, 2177 (1984).
- [3] L. Jacobs, J. V. José, M. A. Novotny and A. M. Goldman, Europhys. Lett. **3**, 1295 (1987).
- [4] L. Jacobs, J. V. José, M. A. Novotny and A. M. Goldman, Phys. Rev. B **38**, 4562 (1988).
- [5] S. Kim and M. Y. Choi, Phys. Rev. B **41**, 111 (1990).
- [6] R. Fazio and G. Schön, Phys. Rev. B **43**, 5307 (1991).
- [7] M. V. Simkin, Phys. Rev. B **44**, 7074 (1991).
- [8] D. Ariosa and H. Beck, Phys. Rev. B **45**, 819 (1992).
- [9] E. Granato and M. A. Contentino, Europhys. Lett. **18**, 343 (1992).
- [10] E. Granato and M. A. Contentino, Phys. Rev. B **48**, 15977 (1993).
- [11] E. Roddick and D. Stroud, Phys. Rev. B **48**, 16600 (1993).
- [12] J. V. José and C. Rojas, Physica C **203**, 481 (1994).
- [13] E. Simanek, *Inhomogeneous Superconductors* (Oxford University Press, New York, 1994).
- [14] B. J. Kim and M. Y. Choi, Phys. Rev. B **52**, 3624 (1995).
- [15] C. Rojas and J. V. José, Phys. Rev. B **54**, 12361 (1996).
- [16] C. Rojas, Ph. D. Thesis, Northeastern University (1995).
- [17] T. K. Kópec and Jorge V. José, Phys. Rev. Lett. **84**, 749 (2000), *ibid* Phys. Rev. **B60**, 7473 (1999).
- [18] L. Capriotti, A. Cuccoli, A. Fubini, V. Tognetti, and R. Vaia, Phys. Rev. Lett. **91**, 247004 (2003).
- [19] L. Capriotti, A. Cuccoli, A. Fubini, V. Tognetti, and R. Vaia, arXiv:cond-mat/0401030, (2004).
- [20] Proceedings of the NATO advanced Research Workshop on Coherence on Superconducting Networks, Delft Netherlands, 1987, Ed. J. E. Mooij and G. B. Schön, Physica B **152**, 1 (1988). Proceedings of the second CTP Workshop on Statistical Physics: KT Transition and Superconducting Arrays, Ed. D. Kim et. al. (Min Eum Sa, Seoul Korea, 1993).
- [21] E. Mooij, B. J. van Wess, L. J. Geerlings, M. Peters, R. Fazio and G. Schön, Phys. Rev. Lett. **65**, 645 (1990).
- [22] H. S. J. van der Zant, Ph. D. Thesis, Delft University (1991).

- [23] H. S. J. van der Zant, L. J. Geerlings and J. E. Mooij, Europhys. Lett. **19**, 541 (1992).
- [24] T. S. Tighe, M. T. Tuominen, J. M. Hergenrother and M. Tinkhman, Phys. Rev. B **47**, 1145 (1993).
- [25] R. Fazio and H. van der Zant, Physics Reports, **355**, 235 (2001), - cond-mat/0011152.
- [26] L. L. Sohn, J. Romijn, E van der Drift, W. J. Elion, and J. E. Mooij, Physica **B194-196**: 125 (1994).
- [27] Y. Takahide, R. Yagi, A. Kanda, Y. Ootuka, and S. Kobayashi, Phys. Rev. Lett. **85**, 1974 (2000).
- [28] D. B. Haviland, K. Anderson, and P. Agren, J. Low Temp. Phys. **118**, 733 (2000).
- [29] P. Delsing, C. D. Chen, D. V. Haviland, Y. Harada and T. Claeson, Phys. Rev. B **50**, 3959 (1994).
- [30] W. J. Elion, Ph. D. Thesis, Delft University (1995).
- [31] H. S. J. van der Zant, W. J. Elion, L. J. Geerlings and J. E. Mooij, Phys. Rev. B **54**, 10081 (1996).
- [32] W. J. Ellison, M. Matters, U. Geigenmüller and J. E. Mooij, Nature, **371**, 594 (1994).
- [33] C. Rojas, J. V. José, and A. M. Tikofsky, Bull. Am. Phys. Soc. **40**; p.68, B11-7 (1995).
- [34] Ya. M. Blanter and G. Schön, Phys. Rev. B **53**; 14534 (1996).
- [35] J. V. José, Jour. Stat. Phys. **93**, 943 (1998).
- [36] J. V. José, L. P. Kadanoff S. Kirkpatrick, and D. R. Nelson, Phys. Rev. B **16**, 1217 (1977).
- [37] H. Kleinert, *Path Integrals in Quantum Mechanics Statistics and Polymer Physics*, (World Scientific, Singapore, 1990).
- [38] H. Flyvbjerg and H. G. Peterson, Jour. Chem. Phys. **91**, 461 (1989).
- [39] P. Minnhagen and P. Olsson, Physica Scripta **46**, 97 (1992); L. Xu and P. Minnhagen, Physica C **218**, 94 (1993).
- [40] V. L. Berezinskii, Zh. Teor. Fiz. **61**, 1144 (1971); J. M. Kosterlitz and D. J. Thouless, J. Phys. **C6**, 1181 (1973); J. M. Kosterlitz J. Phys. **C7**, 1046 (1974).

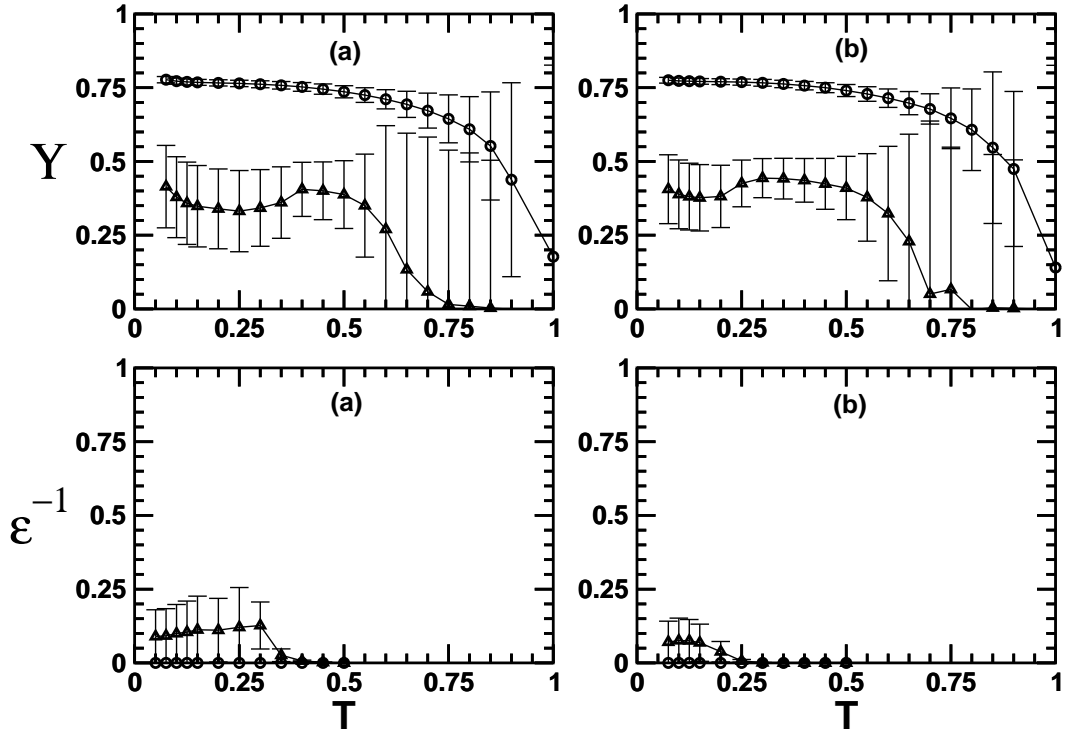


FIG. 1: Υ and ϵ^{-1} as a function of temperature. $\alpha_1 = 0.5$ (circles), for the semiclassical array, and $\alpha_2 = 2.5$ (triangles), for the quantum array. The values of $\frac{C_{\text{int}}}{C_{\text{m}}}$ are (a) 0.52174 and (b) 0.78261.

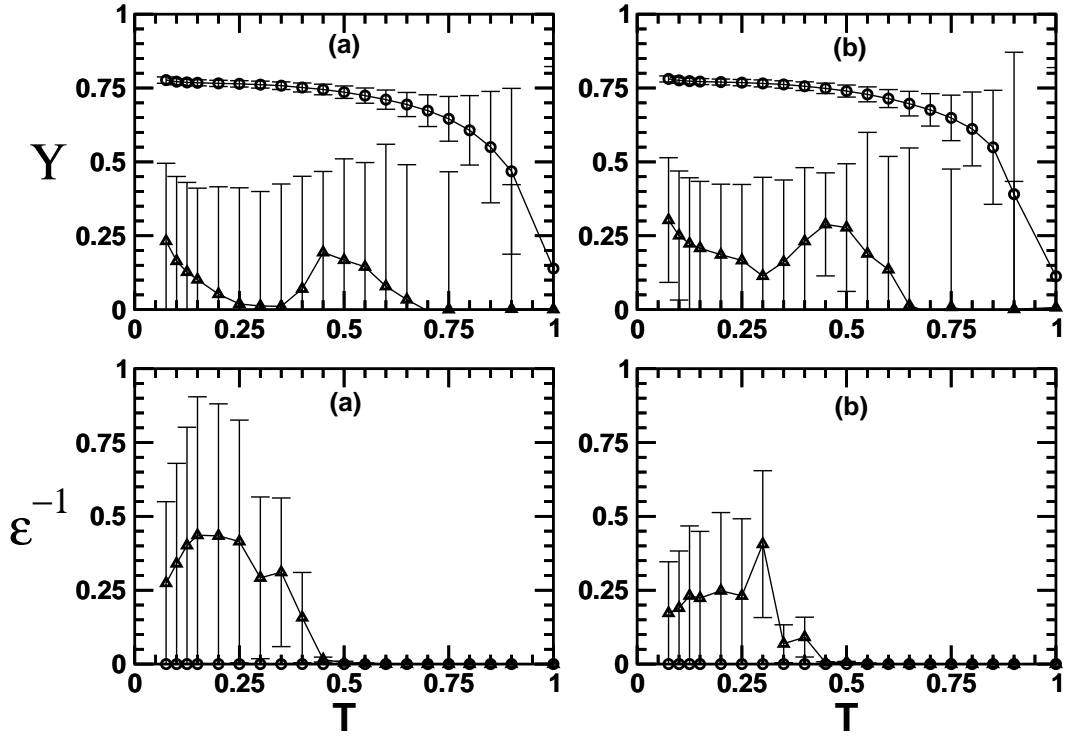


FIG. 2: Same as in Fig. 1 with $\alpha_2 = 3.0$ and $\frac{C_{\text{int}}}{C_{\text{m}}} =$ (a) 0.52174 and (b) 0.78261.

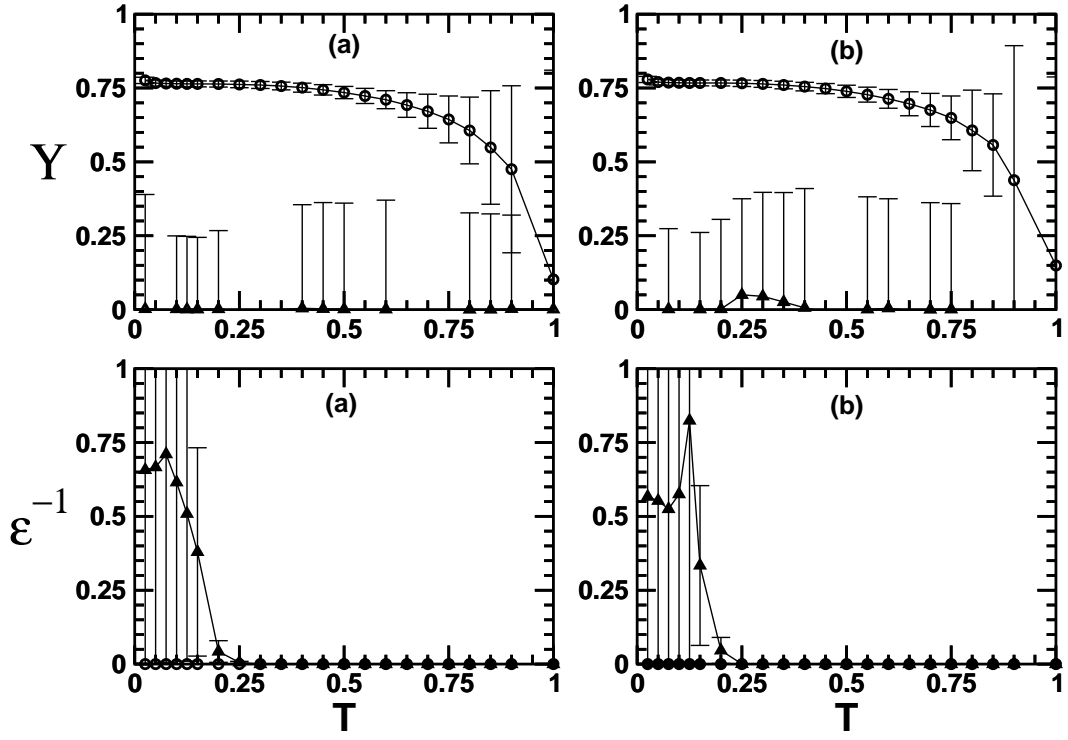


FIG. 3: Same as in Fig. 1 with $\alpha_2 = 4.0$ and $\frac{C_{\text{int}}}{C_{\text{m}}} =$ (a) 0.52174 and (b) 0.78261.

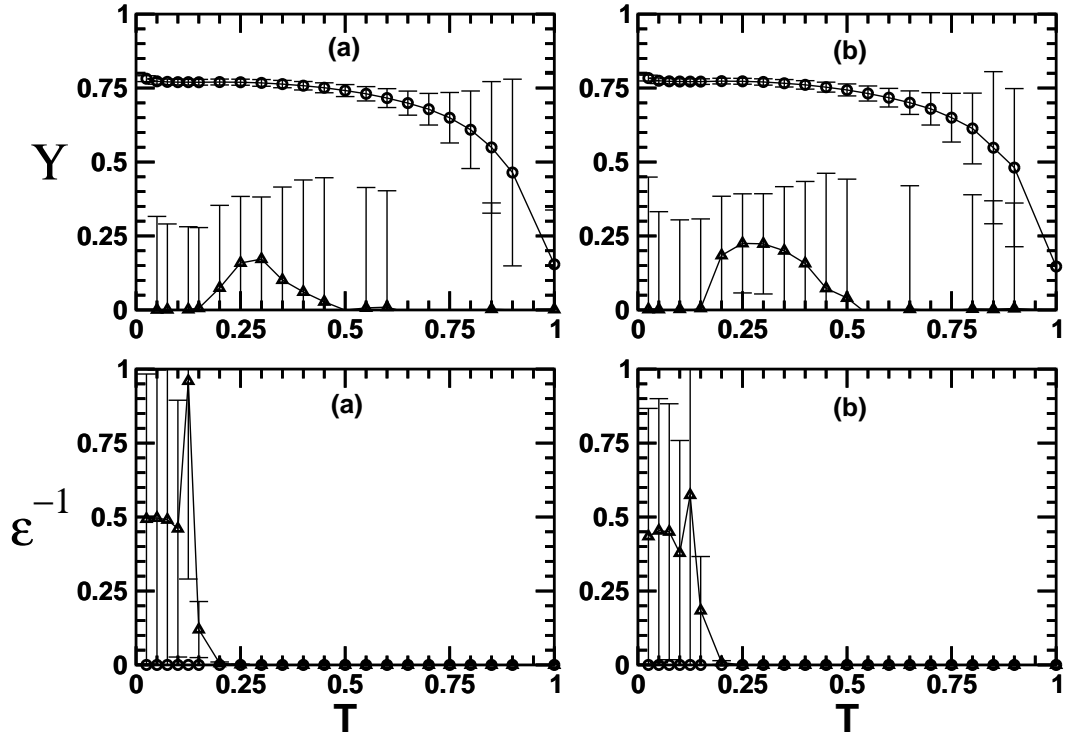


FIG. 4: Same as in Fig. 3 with $\frac{C_{\text{int}}}{C_m}$ (a) 1.04348 and (b) 1.30435.

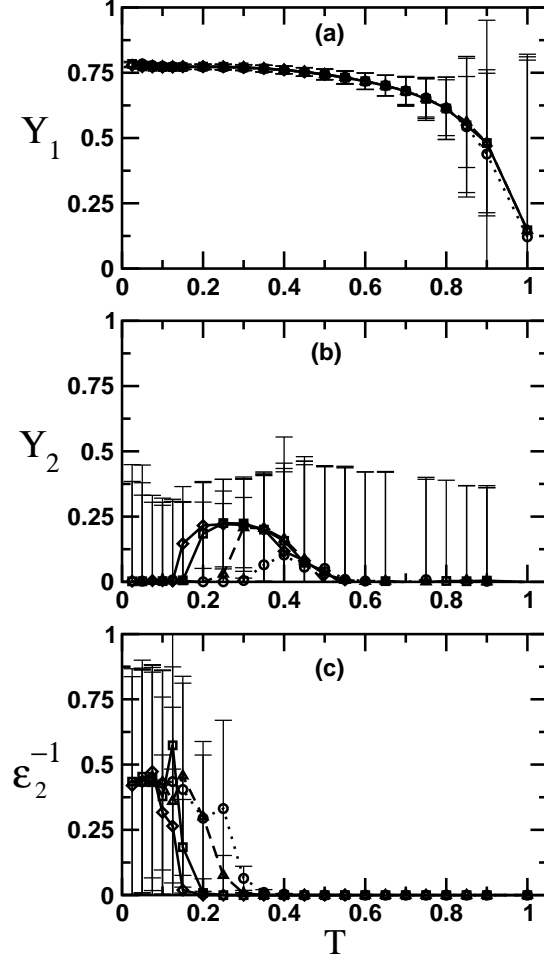


FIG. 5: L_τ finite size behavior of $\Upsilon_{1,2}$ and ϵ_2^{-1} for $L_\tau = 48$ (circles), $L_\tau = 64$ (triangles), $L_\tau = 96$ (squares), and $L_\tau = 128$ (diamonds). The interaction between arrays is $\frac{C_{\text{int}}}{C_{\text{m}}} = 1.30435$. (a) semi-classical array ($\alpha_1 = 0.5$), (b) and (c) quantum array ($\alpha_2 = 4.0$). ϵ_1^{-1} is equal to zero in the whole temperature range and is not shown.

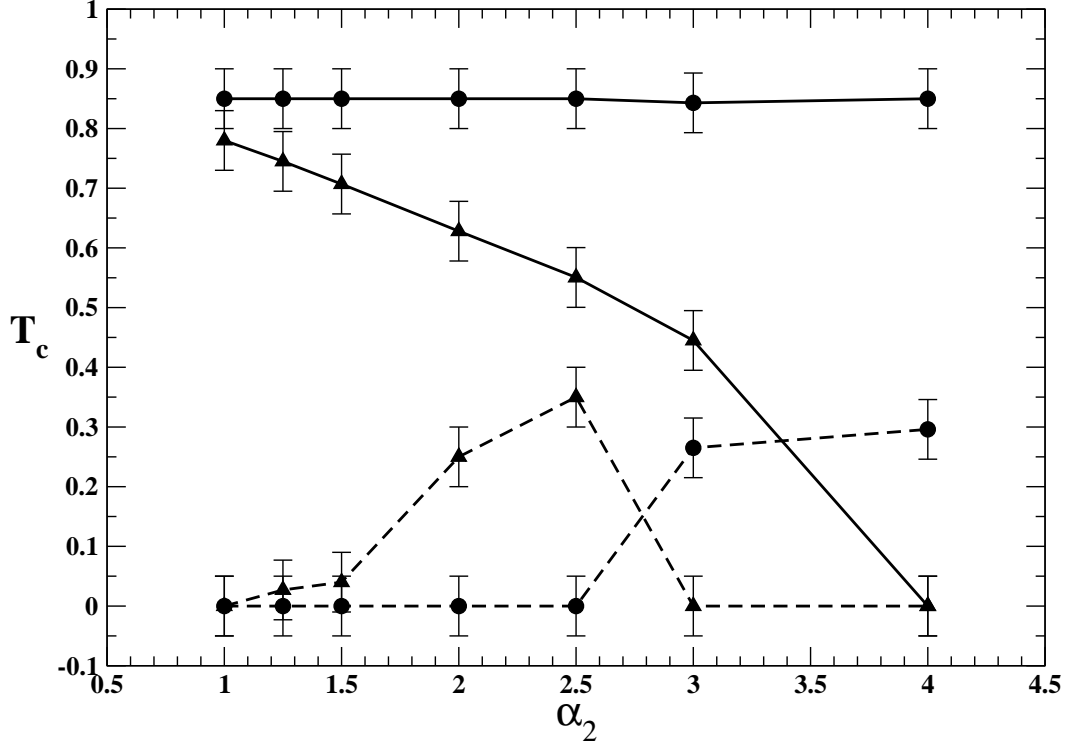


FIG. 6: Estimated transition temperatures of each array versus α_2 for $\frac{C_{int}}{C_m} = 0.52174$. Array 1 (\bullet), array 2 (\blacktriangle). The solid lines represent the SC-N phase boundary while the dashed lines the I-N phase boundary.

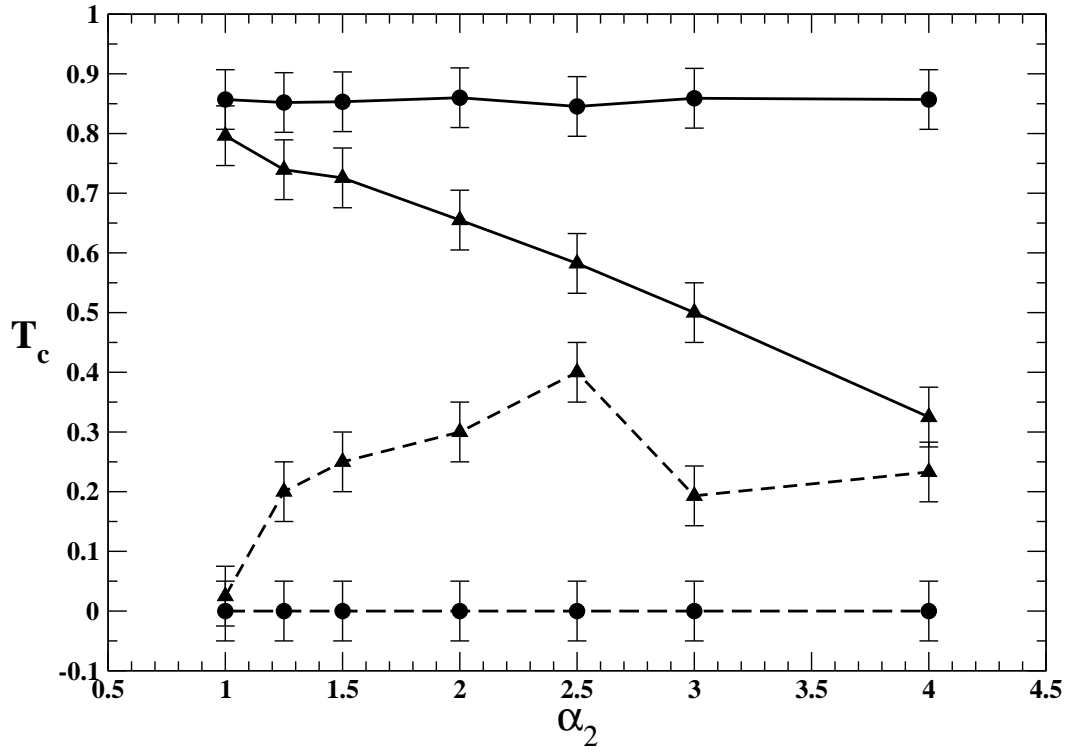


FIG. 7: Same as in Fig. 6 with $\frac{C_{\text{int}}}{C_{\text{m}}} = 1.04348$.

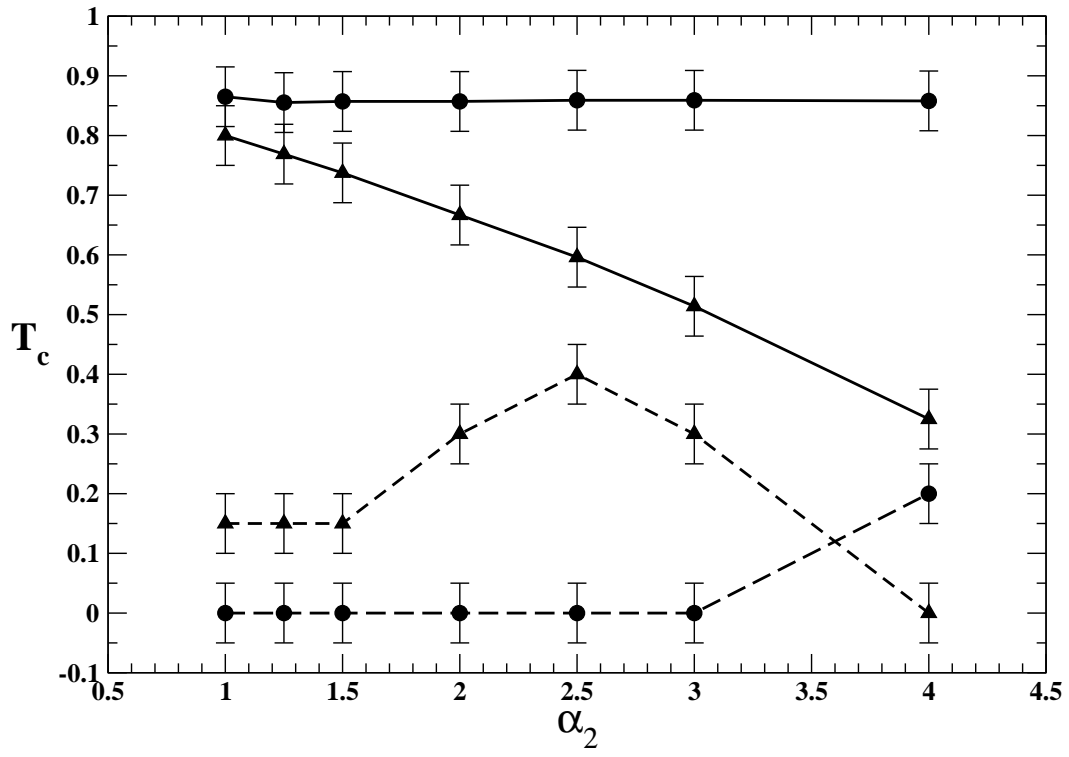


FIG. 8: Same as in Fig. 6 with $\frac{C_{\text{int}}}{C_{\text{m}}} = 1.30345$.